Raman scattering of ferroelectric $Sr_{1-x}Ca_xTiO_3$, x=0.007

1994 J. Phys.: Condens. Matter 6 1229

(http://iopscience.iop.org/0953-8984/6/6/025)

J. Phys.: Condens. Matter 6 (1994) 1229–1238. Printed in the UK

Raman scattering of ferroelectric $Sr_{1-x}Ca_xTiO_3$, $x = 0.007$

U Bianchi†, W Kleemann† and J G Bednorz‡

† Angewandte Physik, Universität Duisburg, 47048 Duisburg, Germany

‡ IBM Research Laboratory, 8803 Rüschlikon, Switzerland

Received 27 October 1993

Abstract. First-order Raman scattering of A_{1g} and E_g modes originating from the antiferrodistortive F_{2u} soft mode confirms the cubic–tetragonal (O_h–D_{4h}) phase transition in $Sr_{0.993}Ca_{0.007}TiO_3$ at $T_0 = 125$ K. Within the cubic and the tetragonal phase first-order Raman scattering of the soft ferroelectric F_{1u} mode (TO_1) and of the hard TO_2 and TO_4 optic modes evidences the existence of Ca^{2+}-centred polar microregions. Their size increases rapidly on cooling towards the ferroelectric ordering temperature, $T_c = 18$ K. Splitting and incomplete softening of the F_{1u} components is consistent with an order–disorder transition into an orthorhombic low-temperature phase with C_{2v} symmetry.

1. Introduction

The well known quantum paraelectric $SrTiO_3$ [1] is very sensitive to doping with impurities. Substituting a sufficient number of Sr^{2+} ions by Ca^{2+} results in low-temperature ($T < 50$ K) ferroelectric behaviour [2]. As shown by measurements of the dielectric permittivity [2] Ca^{2+} induces a phase transition into xy-type ferroelectricity ordering at concentrations $x > x_{cr} = 0.0018$. As in the cases of the related impurity systems $KTaO_3$:Li (KTL) and $KTaO_3$:Nb (KTN) [3], it is assumed that the Ca^{2+} impurity ions, which are smaller in size than the substituted ones ($r_{Ca}/r_{Sr} \simeq 0.9$), occupy off-centre positions at the Sr^{2+} sites. Within a structurally single-domained sample one finds weak secondary anisotropy with easy axes along the cubic ⟨110⟩ directions [2]. Rounding of the dielectric permittivity peaks, ϵ' against T, at $x > 0.016$ [2], field-switchable linear birefringence [4] and polydispersive domain wall permittivity [5] are attributed to a random-field (RF)-induced ferroelectric domain state [6]. The RFs are very probably [2, 4] caused by randomly distributed Ca^{2+}–V_0 centres substituting Ti^{4+}–O^{2-} ion pairs.

Because of the highly polarizable host lattice any polar dopant induces ferroelectric microordered regions (FMR) at high temperatures prior to the global long-range ordering at low temperatures [7, 8]. Ferroelectrically ordered clusters grow on cooling and mediate first-order Raman scattering of the ferroelectric soft mode TO_1 (F_{1u} in cubic symmetry) resulting in a broad precursor band. The shape of this band reflects the distribution of relaxation frequencies of the FMRs and allows for an estimate of their spatial extension [8, 9].

In this investigation we report on the scattering band due to Ca^{2+}-centred FMRs in $Sr_{1-x}Ca_xTiO_3$ ($x = 0.007$), henceforth denoted as SrCaT. We determine its frequency shift at various temperatures, T, and estimate the spatial extensions of the FMRs by fitting to theoretical predictions [8, 9]. In addition, the $2TO_1$ resonance band is observed as in pure $SrTiO_3$ [10]. Hard polar modes, such as TO_2 and TO_4, are also influenced by the relaxational frequencies of the FMRs. For KTL and KTN [9, 11], the corresponding Raman scattering lines show a typical asymmetry, which was also looked for in SrCaT.

0953-8984/94/061229+10$07.50

The transition from the tetragonal to the orthorhombic phase at T_c gives rise to first-order Raman scattering and splitting of the ferroelectric soft mode TO_1 into three components. Additionally, the degeneracy of the E_g-type structural soft mode is removed by splitting at $T < T_c$. It originates, as well as the A_{1g}-type structural soft mode, from the antiferrodistortive soft F_{2u} zone boundary phonon, which becomes Raman active below the cubic–tetragonal transition temperature, $T_0 = 125$ K. Preliminary results have been presented previously [12].

2. Experimental procedure

The Raman scattering experiments were done on a single-crystal sample with dimensions $0.8 \times 1.0 \times 3.6$ mm^3 along the cubic directions $[110]_c = a$, $[1\bar{1}0]_c = b$, and $[001]_c = c$, respectively. The spectra were recorded with a Jobin–Yvon U-1000 double monochromator ($f = 1$ m) after excitation with 100 mW Ar^+ laser light ($\lambda = 488$ nm) in 90° scattering geometries, $z(ij)x$, with $x \parallel a$, $y \parallel b$, $z \parallel c$ and $i \parallel a$, or b, $j \parallel b$ or c. Here a, b and c denote the tetragonal (orthorhombic) axes at $T_c < (T < T_c)$. As checked by polarizing microscopy a nearly perfect tetragonal single domain is formed at $T < T_0$ and is described by the above notation. At $T < T_c$, however, a and b are interchanging between adjacent stripe domains stacked along the c axis with average thickness $d \simeq 10$ μm [12].

$T_0 = 125$ K was obtained from measurements of the principal ac birefringence. This value served to determine the actual Ca^{2+} concentration of the sample, $x = 0.007$, when comparing with T_0 obtained previously for various other samples with the birefringence technique [4]. The result compares well with dielectric permittivity data [13], which yield a peak temperature $T_m = 17.6$ K of ϵ' and, hence, $x = 0.0053$ according to Bednorz and Müller's interpolation formula of T_m versus x [2]. Henceforth we shall use the x value determined by birefringence. We believe it to be more accurate because of the linear dependence of T_0 on x and the much larger variation of T_0 than T_c with x.

The crystal was polished to optical quality on all faces. The two ac faces were covered with gold electrodes by vacuum deposition for experiments with external electric fields. Assuming that Raman scattering probes bulk properties of the crystal, we did not remove surface stress layers [14]. However, chemical etching proved to be necessary for dielectric permittivity measurements [2, 13]. All measurements were temperature controlled to within $\delta T \sim \pm 0.05$ K at $5 \leqslant T \leqslant 300$ K by means of a gas flow cryostat.

3. Experimental results and discussion

Figure 1 shows the Raman spectra of SrCaT with Raman shifts up to $\Delta\omega = 1000$ cm^{-1} at various temperatures between 10 and 300 K without analysing the scattered light. The room-temperature spectrum is a pure second-order spectrum because of the cubic symmetry (O_h) of the parent phase. It consists mainly of three scattering bands. The two bands with the larger shifts, centred at 300 cm^{-1} and 650 cm^{-1}, respectively, are superpositions of different combination modes [15]. The scattering band lying at $\Delta\omega = 73.5$ cm^{-1} is attributed to the TO_2–TO_1 or TO_2–TA difference modes (see also figure 2). Upon lowering the temperature this difference band gradually disappears. It is nearly invisible at about 100 K, just below the cubic–tetragonal transition temperature $T_0 = 125$ K [12]. Simultaneously the intensity of two high-frequency second-order scattering bands strongly decreases. According to the tetragonal symmetry below T_0 two hard modes appear at 145 cm^{-1} (E_g) and at 450 cm^{-1}

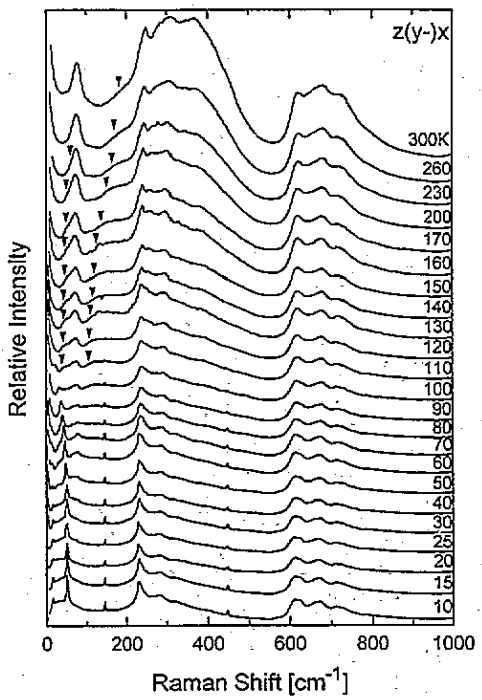

Figure 1. $z(y-)x$ Raman spectra of SrCaT ($x = 0.007$) recorded up to 1000 cm^{-1}. Arrowheads indicate the peak positions of the $2TO_1$ and TO_1-like FMR scattering bands. Temperatures between 10 K and 300 K are increasing from bottom to top.

(B_{1g}). Closer inspection of the 145 cm^{-1} line in more resolved spectra (figure 2) reveals a vanishing shift on lowering T. This seems to hint at a vanishing Grüneisen parameter of this mode.

With the transition to tetragonal symmetry the degeneracy of the antiferrodistortive F_{2u} soft mode is removed and two lines become Raman active. These lines are the A_{1g} (figure 2(a), (d)) and the E_g (figure 2(b), (c)) structural soft modes ($\Delta\omega = 52$+cm^{-1} and 14 cm^{-1}, respectively, at $T = 5$ K). They harden upon cooling, thus reflecting the gradual increase of the rotation angle of the oxygen octahedra around the c axis. The variation with T of their peak positions is shown in figure 3.

Two scattering bands (figures 1 and 2, arrowheads) appear below 250 cm^{-1} with decreasing Raman shift as the temperature is lowered. In previous experiments on pure $SrTiO_3$ [8, 10] these bands were also observed. The lower-frequency band was attributed to first-order Raman scattering of the ferroelectric TO_1 soft mode activated by FMRs [8]. The higher-frequency band is due to second-order Raman scattering of a two-phonon resonance state of the ferroelectric soft mode, $2TO_1$ [10]. Within errors, the frequencies of the low-energy shoulders of these two bands vary nearly perfectly with T as the frequency and twice its value, respectively, of the TO_1 ferroelectric soft mode. This is shown in figure 3, where the frequencies of FMR Raman scattering are compared with data of the ferroelectric soft mode behaviour obtained from neutron (full squares) [16] and field-induced Raman scattering experiments (full circles) [17] on pure $SrTiO_3$ as a function of T. Only at low temperatures, $T < 30$ K, does the FMR frequency fall below that of TO_1 in pure $SrTiO_3$. This is due to the interaction between soft mode and cluster vibrations similar to that observed in KTN [18]. The eventual conversion into symmetry-allowed first-order scattering and the line splitting observed at $T < 18$ K will be discussed below.

A simple theory [7] describes the frequency-dependent scattering intensity of the low-frequency band (FMR) assuming spherical regions with ferroelectric ordering embedded in

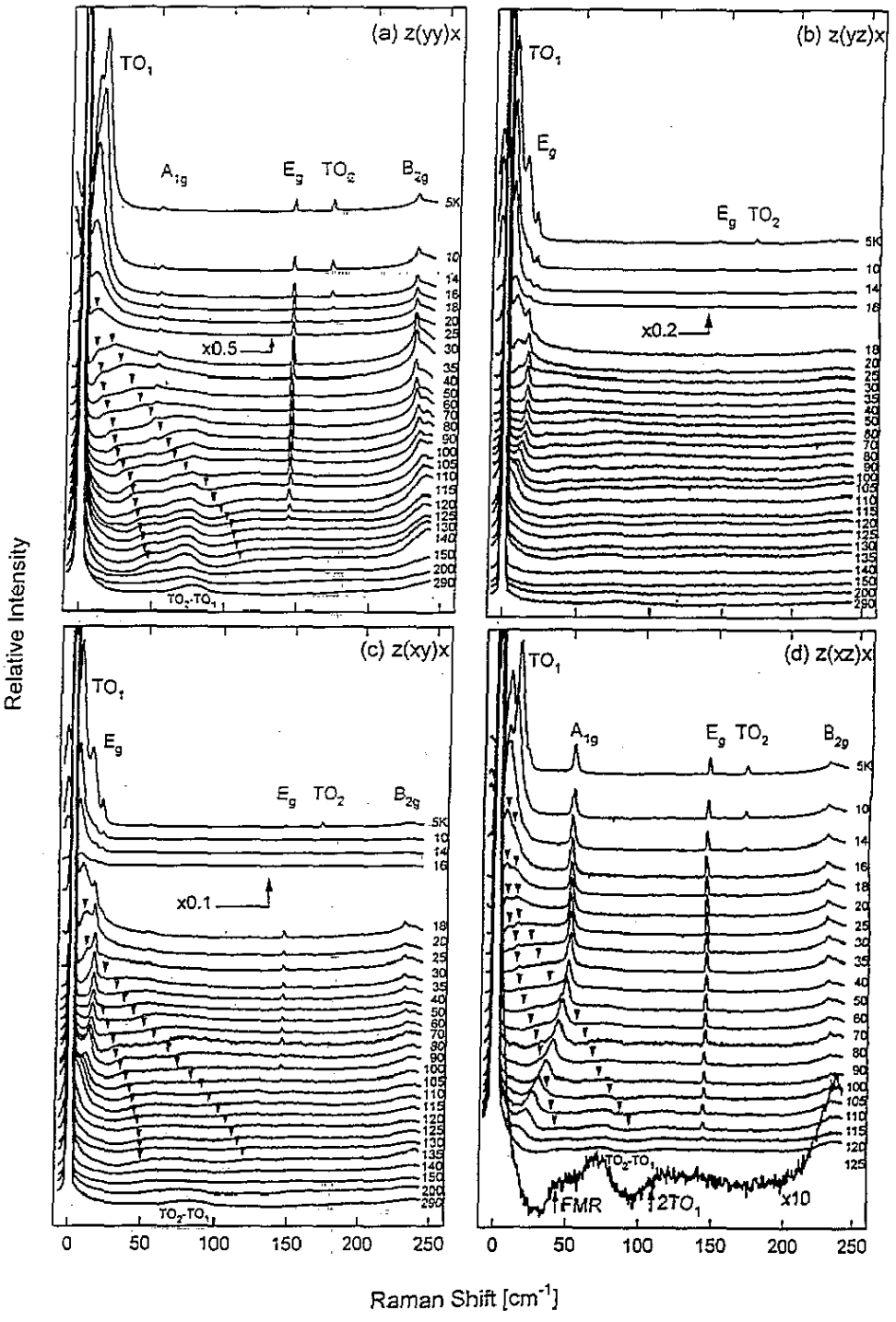

Figure 2. Raman spectra of SrCaT ($x = 0.007$) recorded up to 250 cm^{-1} in scattering geometries (a) $z(yy)x$, (b) $z(yz)x$, (c) $z(xy)x$ and (d) $z(xz)x$. The TO_1-like FMR and the $2TO_1$ scattering bands (arrowheads), the structural soft modes E_g and A_{1g}, the structural hard mode E_g, the difference mode TO_2–TO_1 and the polar hard mode TO_2 are indicated. Temperatures are decreasing from bottom to top.

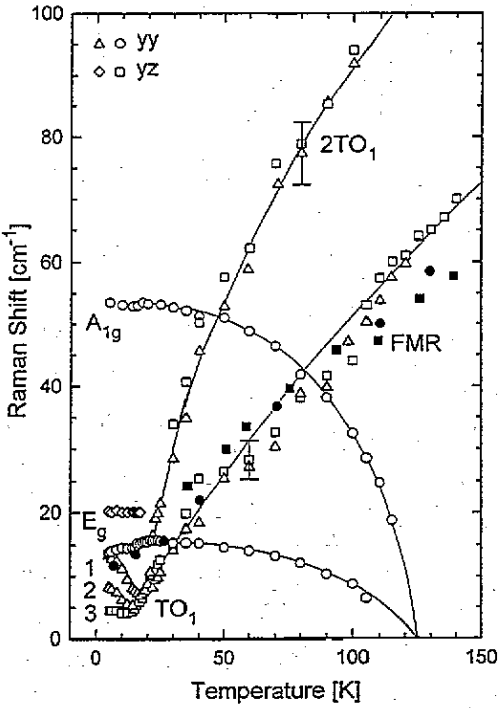

Figure 3. Peak positions of various soft modes (see figure 2) versus temperature connected by eye-guiding solid lines observed for SrCaT (x = 0.007) in $z(yy)x$ and $z(yz)x$ scattering geometries. Solid symbols refer to field-induced Raman [17] (circles) and neutron scattering [16] experiments (squares) on pure $SrTiO_3$.

the cubic or tetragonal host lattice. The cluster-size-dependent line shape of the scattering intensity is expressed as

$$I(\omega) \propto \{1/[1-\exp(-\hbar\omega/kT)]\} K Q/(K^2+Q^2)^2 \qquad (1)$$

with

$$K = a/2\pi R_0 \qquad Q^2 = a^2 q_\omega^2/(2\pi)^2 = (a/2\pi)^2[\omega^2 - \omega_0(T)^2]/D^2.$$

a = 0.39 nm is the lattice constant, D describes the phonon dispersion and is for simplicity assumed to be isotropic with a temperature-independent value of 100 meV as proposed for $KTaO_3$ [7] (expressing q_ω in reduced units, equal to 0.5 at the zone boundary) and R_0 is the cluster radius. $\omega_0(T)$ is the temperature dependent value of the soft mode frequency.

In order to estimate R_0 values we have evaluated the $z(yy)x$ spectra between T = 18 and 23 K as shown in figure 4(a). The pure FMR Raman lines are approximately given by I versus $\Delta\omega$ curves between $\Delta\omega$ = 5 and 15 cm^{-1}. Within this range the overlap with the quasi-elastic (QE, $\Delta\omega \sim 0$) and the $2TO_1$ scattering lines, respectively, seems to be negligible. A best three-parameter fit of the experimental data within these limits to (1) yields $R_0(T)$, $\omega_0(T)$ and an amplitude factor.

The fitted soft-mode frequencies, $\omega_0(T)$, are systematically smaller by about 6 cm^{-1} than the peak positions of the FMR bands as shown in figure 3. the $R_0(T)$ values increase steeply from 3.7 to 8.4 nm within the T interval from 23 to 18 K. As can be seen in figure 5 the growth of the clusters appears to be near-critical when approaching T_c = 18 K. However, a best fit to a correlation-length type critical power law, $R_0(T) \propto (T/T'-1)^\nu$ (solid line in figure 5), yields parameters T' = 4.9 K and ν = 2.4, which are far from the expected ones, $T' \sim T_c$ = 18 K and $\nu \sim 0.5$. In accordance with theoretical prediction [3] the T dependence

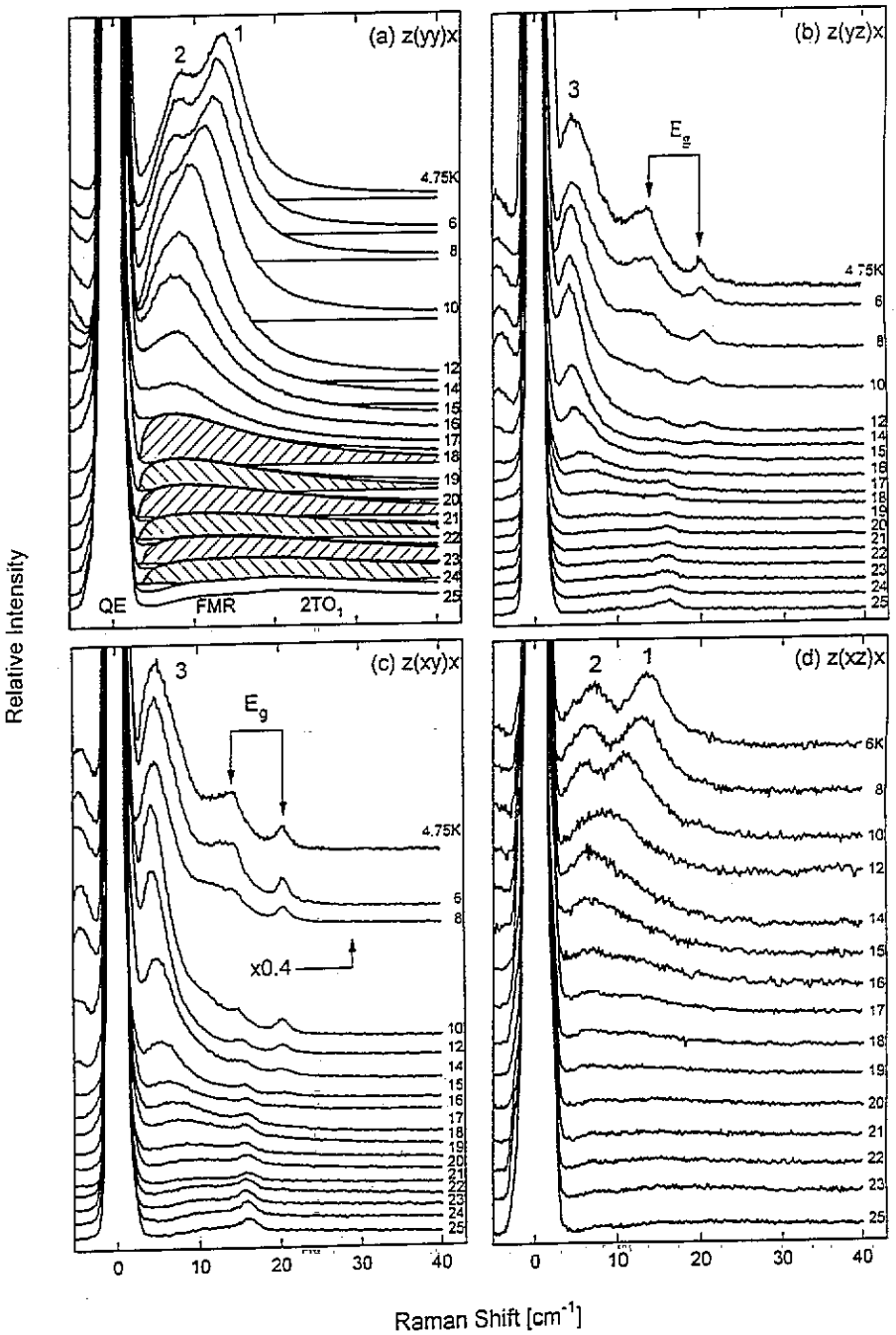

Figure 4. Low-frequency ($\Delta\omega < 40$ cm^{-1}) and low-temperature ($T < 25$ K) Raman spectra of SrCaT ($x = 0.007$) in scattering geometries (a) $z(yy)x$, (b) $z(yz)x$, (c) $z(xy)x$ and (d) $z(xz)x$, showing the splittings of the cubic F_{1u} ferroelectric soft mode into three components (denoted 1, 2 and 3) and of the structural E_g soft mode. The positions of the quasi-elastic (QE), FMR and $2TO_1$ lines are indicated. In (a) theoretical FMR lines by fitting I versus $\Delta\omega$ within $5 \leqslant \Delta\omega \leqslant 15$ cm^{-1} to (1) are depicted by hatched areas for $18 \leqslant T \leqslant 23$ K. TO_1 base lines for $T \leqslant 14$ K are indicated.

of R_0 rather marks a non-critical percolative transition. In fact, when considering the average Ca^{2+}–Ca^{2+} distance at $x = 0.007$, $d \sim 3.0$ nm, the clusters are expected to touch each other and induce ferroelectricity [3] as $R_0(T) \rightarrow d$. This simple argument in conjunction with the data of figure 5 yields $T_c \sim 23$ K in poor agreement with the observed [12] value, $T_c = 18$ K. Better agreement is expected when refining the evaluation of the FMR scattering spectra. For example, (1) neglects the well known cluster shape anisotropy. It is assumed [8] that SrCaT forms ellipsoidally shaped clusters, as was found in KTL [19]. In the near future we hope to obtain more insight into the pre-transitional cluster dynamics and the ferroelectric percolation transition by fitting to recent more sophisticated theory [9, 11]. In particular, the transition from quasi- to real first-order Raman scattering needs clarification. Moreover, the discrepancy between $\omega_0(T)$ as obtained from the low-energy shoulder and the first moment of the TO_1 line above and below T_c, respectively, is expected to vanish when taking into account finite damping [11]. The new theory could thus improve the fit, but useful physics is already contained in the above treatment. It considers that the spectra are easily described as the result of 'first-order' scattering induced by the structure factor of the FMRs.

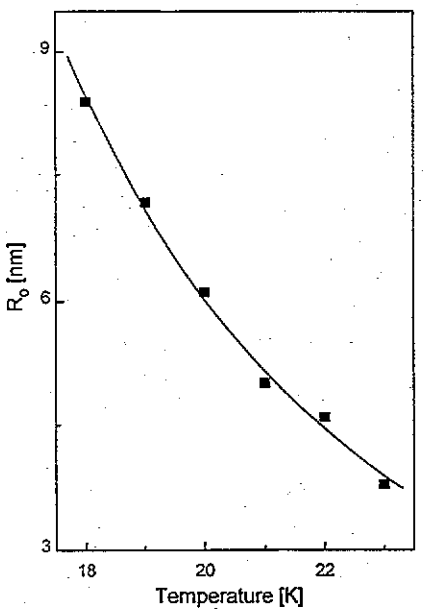

Figure 5. Radius R_0 of ferroelectric clusters versus T obtained from best fits of FMR line shapes between $\Delta\omega$ = 5 and 15 cm^{-1} (figure 4(a)) to (1).

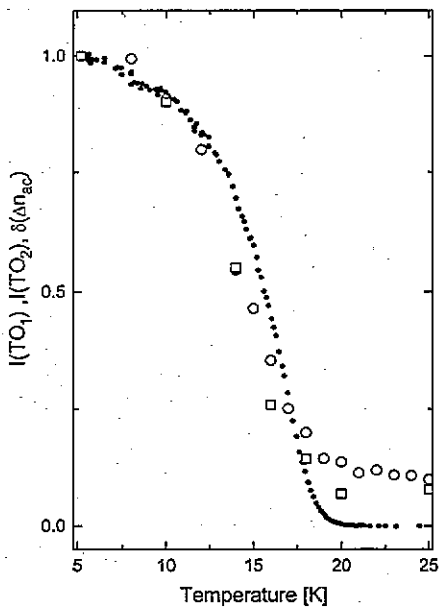

Figure 6. Normalized temperature dependence of the integrated intensities of the TO_1 (figure 4(a), corrected for the Bose factor, open circles) and TO_2 modes (open squares) and of normalized $\delta(\Delta n_{ac})$ (solid circles).

The integrated intensity of the FMR band, $I(TO_1)$, increases rapidly below T_c, where it converts into the first-order TO_1 scattering line. This is seen in all scattering geometries in figure 2 and (in more detail) figure 4. Figure 6 shows $I(TO_1)$ versus T obtained from spectra in $z(yy)x$ geometry by integrating between the minimum adjacent to the QE line and 25 cm^{-1} ($2TO_1$ cut-off) and correcting for the Bose factor, $(1-\exp(-\hbar\omega/k_BT))^{-1}$. Similarly as argued for the polar hard mode intensities, $I(TO_2)$ and $I(TO_4)$ [11], the data reflect the T dependence of the autocorrelation function $\langle P^2 \rangle$ of the spatially (r) and temporally

(t) fluctuating impurity-induced polarization $P(r, t)$. Proportionality with the morphic contribution to the principal birefringence, $\delta(\Delta n_{ac})$, is expected [4, 12]. This is roughly confirmed for both $I(TO_1)$ and $I(TO_2)$ (obtained from figure 7, see below) as shown in figure 6.

Global breaking of the inversion symmetry accompanied by long-range structural distortion is evident from the splitting of the TO_1 line at $T < T_c$. We find three components, denoted 1, 2 and 3 in figure 4. They continue to soften, however, and reach minimal energies at surprisingly different temperatures (figure 3). The highest-energy component 1 dominates the $z(yy)x$ spectrum (figure 4(a)). Upon cooling it softens to $\Delta\omega = 7$ cm^{-1} at $T = 18$ K and then hardens to $\Delta\omega = 13$ cm^{-1} at $T = 5$ K. The other two components split off at $T = 15$ K, where $\Delta\omega = 5.5$ cm^{-1}. The component 2 is visible in the $z(yy)x$ and $z(xz)x$ configurations (figure 4(a) and (d)) and hardens to $\Delta\omega = 8.5$ cm^{-1} at $T = 5$ K. The component 3 is visible only in the non-diagonal scattering geometries $z(yz)x$ and $z(xy)x$ (figure 4(b) and (c)). It softens with decreasing T to a minimal shift $\Delta\omega = 4$ cm^{-1} at $T = 10$ K and then hardens to $\Delta\omega = 5$ cm^{-1} at $T = 5$ K.

According to the definition of the crystal axes given above the 'hardest' components 1 and 2 presumably correspond to the $B_1(x)$ and $B_2(y)$ modes in C_{2v} point group symmetry [20], whereas component 3 is presumably due to the $A_1(z)$ mode. At this point one should remember that the crystal subdivides into domains [12] with alternating a and b axes in the ferroelectric phase. Hence different scattering geometries are probed simultaneously and sharp selection rules are lacking.

The observed softening of the TO_1 components below T_c clearly rules out a displacive-type phase transition in SrCaT. This is reminiscent of the behaviour of KTN, where the minimal soft-mode energy is, however, attained at temperatures above T_c [18]. Very probably both of these systems have to be considered as order–disorder-type percolative ferroelectrics. The unusual softening at $T < T_c$ in SrCaT hints in particular at a certain independence of the dynamics of the host crystal from the criticality of the cluster percolation.

The temperature $T \sim 18$ K, where the first splitting takes place, coincides with the sharp onset of morphic ab linear birefringence ($a = b$ in the tetragonal phase) [12] and the peak of the dielectric in-plane permittivity, ϵ' versus T [13]. More accurately, these quantities define the phase transition temperature as $T_c = 17.6$ K.

Below $T_c = 18$ K another new line appears at $\Delta\omega = 20$ cm^{-1} (figures 3 and 4). Simultaneously the structural E_g soft mode shifts from $\Delta\omega \simeq 16$ cm^{-1} to 14 cm^{-1}. Very probably, the doubly degenerate structural E_g mode splits into two components owing to the tetragonal–orthorhombic lattice distortion. It is noticed that the structural A_{1g} mode ($\Delta\omega = 52$ cm^{-1}) also slightly softens at $T < T_c$ (figure 3). This might indicate spontaneous dilation along c in the orthorhombic phase.

The temperature dependences of the hard polar modes TO_2 ($\Delta\omega = 171$ cm^{-1}) and TO_4 (545 cm^{-1}) are shown in figure 7 for various temperatures between 6 and 20 K. In accordance with theory [9, 11] both of these modes are mediated by FMRs in the paraelectric phase, $T > T_c$. The precursor region is less extended than in KTL, but rather resembles that of KTN [9, 11]. This hints at high relaxational frequencies of the off-centre Ca^{2+} dipoles [11]. In fact, similar to the situation found for the highly mobile Nb^{5+} off-centre dipoles in KTN [21] the dielectric dispersion step due to dipolar cluster relaxation in SrCaT is found to lie beyond $f = 10^7$ Hz [13]. Previously reported [5] low-frequency dispersion steps at $f \sim 10^4$ Hz were identified [13] as artifacts due to surface impedance effects.

Slight asymmetry of the TO_2 line, tailing off at the high-frequency side, is expected at $T > T_c$ from theory [9, 11]. It is, in fact, visible (figure 7) but hard to evaluate because of

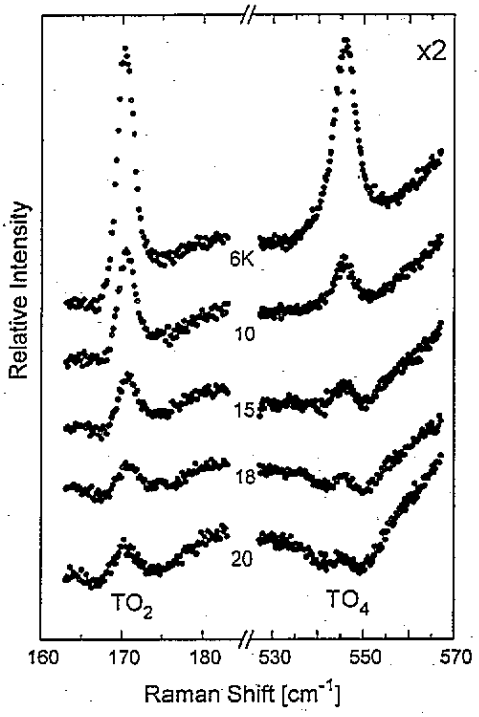

Figure 7. Raman spectra of the polar hard modes TO_2 and TO_4 recorded in $z(yy)x$ geometry at temperatures between 6 and 20 K.

the rapid drop of intensity in the paraelectric phase. Similarly, we were not able to obtain reliable Raman spectra of the non-polar TO_3 hard mode. Very probably it is hidden in the high-frequency slope of the strong B_{2g} line at $\Delta\omega \sim 265$ cm^{-1} (figure 1). The TO_3 mode was successfully used to identify the onset of long-range macroscopic distortion in KTL and KTN [9, 11].

4. Conclusion

Raman scattering data evidence different processes in SrCaT with $x = 0.007$.

(a) The phase transition at $T_0 = 125$ K from the cubic (O_h) parent phase into a tetragonal (D_{4h}) state is evidenced by the appearance of the A_{1g} ($\Delta\omega = 52$ cm^{-1} at $T = 5$ K) and E_g ($\Delta\omega = 14$ cm^{-1} at $T = 5$ K) soft modes and of two hard modes denoted E_g ($\Delta\omega = 145$ cm^{-1}) and B_{1g} ($\Delta\omega = 450$ cm^{-1}).

(b) The phase transition at $T_c = 18$ K from tetragonal (D_{4h}) to orthorhombic (presumably C_{2v}) symmetry is evidenced by

(i) the appearance of Raman scattering of the polar hard modes TO_2 ($\Delta\omega = 172$ cm^{-1}) and TO_4 ($\Delta\omega = 547$ cm^{-1}) and their subsequent increase of intensity.

(ii) the splitting of the ferroelectric cubic F_{1u} soft mode below T_c into three components, which harden (to $\Delta\omega = 5$ cm^{-1}, 8.5 cm^{-1} and 13 cm^{-1} at $T = 5$ K, respectively) and grow appreciably in intensity on further cooling and

(iii) the splitting of the doubly degenerate E_g structural soft mode into two components at T_c ($\Delta\omega = 14$ cm^{-1} and 20 cm^{-1} at $T = 5$ K).

(c) Dipolar ordered clusters with broken inversion symmetry are observed via a precursor Raman scattering band with a shoulder at ω_{TO_1} at temperatures up to $10T_c$. The change of

the shape of the TO_1-like scattering band indicates growth of the ferroelectrically ordered clusters on lowering the temperature. They reach the 10 nm scale and percolate at T_c.

Further investigations are needed in order to understand the observed disconnection of the soft mode dynamics from the percolative transition.

Acknowledgment

This work was supported by the Deutsche Forschungsgemeinschaft via Forschungsschwerpunkt 'Pseudosymmetrische Kristalle'.

References

[1] Müller K A and Burkhard H 1979 *Phys. Rev.* B **19** 3593
[2] Bednorz J G and Müller K A 1984 *Phys. Rev. Lett.* **52** 2289
[3] Vugmeister B E and Glinchuk M D 1990 *Rev. Mod. Phys.* **62** 993
[4] Kleemann W, Schäfer F J, Müller K A and Bednorz J G 1988 *Ferroelectrics* **80** 297
[5] Kleemann W and Schremmer H 1989 *Phys. Rev.* B **40** 7428
[6] For a review see Kleemann W 1993 *Int. J. Mod. Phys.* B **7** 2469
[7] Uwe H, Lyons K B, Carter H L and Fleury P A 1986 *Phys. Rev.* B **33** 6436
[8] Uwe H, Yamaguchi H and Sakudo T 1989 *Ferroelectrics* **96** 123
[9] Toulouse J, DiAntonio P, Vugmeister B E, Wang X M and Knauss L A 1992 *Phys. Rev. Lett.* **68** 232
[10] Sekine T, Uchinokura K and Matsuura E 1976 *Solid State Commun.* **18** 569
[11] DiAntonio P, Vugmeister B E, Toulouse J and Boatner L A 1993 *Phys. Rev.* B **47** 5629
[12] Bianchi U, Kleemann W and Bednorz J G 1993 *Ferroelectrics* at press
[13] Dec J, Bianchi U, Kleemann W and Bednorz J G 1993 in preparation
[14] Aso K 1976 *Japan. J. Appl. Phys.* **15** 1243
[15] Nielsen W G and Skinner J G 1968 *J. Chem. Phys.* **48** 2240
[16] Cowley R A 1964 *Phys. Rev.* **134** A981
[17] Fleury P A and Worlock J M 1968 *Phys. Rev.* **174** 613
[18] Chou H, Shapiro S M, Lyons K B, Kjems J and Rytz D 1990 *Phys. Rev.* B **41** 7231
[19] Stachiotti M G and Migoni R L 1990 *J. Phys.: Condens. Matter* **2** 4341
[20] Uwe H and Sakudo T 1976 *Phys. Rev.* B **13** 271
[21] Fontana M D, Maglione M and Höchli U T 1993 *J. Phys.: Condens. Matter* **5** 1895